Single-electron magnetoconductivity of a nondegenerate two-dimensional electron system in a quantizing magnetic field

Frank Kuehnel,[1] Leonid P. Pryadko,[2,3] and M. I. Dykman[1,*]
[1]*Department of Physics and Astronomy, Michigan State University, East Lansing, Michigan, 48823*
[2]*School of Natural Sciences, Institute for Advanced Study, Princeton, New Jersey, 08540*
[3]*Department of Physics, University of California, Riverside, California, 92521*
(Received 29 August 2000; revised manuscript received 25 January 2001; published 5 April 2001)

We study transport properties of a nondegenerate two-dimensional system of noninteracting electrons in the presence of a quantizing magnetic field and a short-range disorder potential. We show that the low-frequency magnetoconductivity displays a strongly asymmetric peak at a nonzero frequency. The shape of the peak is restored from the calculated 14 spectral moments, the asymptotic form of its high-frequency tail, and the scaling behavior of the conductivity for $\omega \to 0$. We also calculate ten spectral moments of the cyclotron resonance absorption peak, and restore the corresponding (nonsingular) frequency dependence using the continuous fraction expansion. Both expansions converge rapidly with an increasing number of included moments, and give numerically accurate results throughout the region of interest. We discuss the possibility of an experimental observation of the predicted effects for electrons on helium.

DOI: 10.1103/PhysRevB.63.165326 PACS number(s): 73.23.−b, 73.50.−h, 73.43.−f

I. INTRODUCTION

A single-electron dynamics in the lowest Landau level (LLL), broadened by a delta-correlated scalar disorder potential, provides the simplest framework for the analysis of the integer quantum Hall effect (IQHE). Wegner's exact calculation[1] of the density of states raised hopes that the corresponding model may be exactly solvable, and much effort was put into understanding transport in this model. However, in contrast to the density of states, the conductivity is expressed in terms of a two-particle Green's function, and depends not only on the energies of single-particle states, but also on their wave functions.

Nearly all single-electron wave functions of the disorder-broadened Landau levels are localized. The localization length ξ strongly depends on energy. For small energies E counted off from the Landau band center (in the neglect of band mixing), ξ diverges as a universal power[2,3] of $|E|$. These are the large-radius states that form the low-frequency conductivity, because it involves large electron displacements and small energy transfer. As a result, for Fermi energies close to a band center, the conductivity displays a universal critical behavior at sufficiently small temperatures and frequencies.

The width of the critical region depends on the properties of the disorder potential and the Landau-level number. For the lowest Landau level, it is of the order of the bandwidth $\hbar\gamma$, the only dimensional parameter of the Hamiltonian projected on the LLL (we assume that the cyclotron frequency $\omega_c \gg \gamma$). Outside the scaling region, the spatial extent of the eigenstates is small, of the order of the magnetic length $l = (\hbar/m\omega_c)^{1/2}$, and the universality is lost. Therefore, the overall frequency dependence of the conductivity is determined by the disorder mechanism, and may allow one to discriminate between different mechanisms. For this reason, it is interesting to obtain the frequency dependence of the conductivity, including its universal and nonuniversal parts, at least for some basic models of disorder. It is also of interest to find highly accurate numerical results, as they may be used to test various approximate analytical approaches.

In the present paper we consider frequency-dependent conductivity in the single-electron approximation. Motivated by the experiment, and in order to make the problem tractable, we assume that

$$\hbar\gamma \ll k_B T, \quad nl^2 \ll 1, \tag{1}$$

i.e., the disorder-induced broadening of the lowest Landau level is small compared to temperature, and simultaneously the filling fraction is small, so that the electron system is nondegenerate. This parameter range is of interest for several two-dimensional electron systems (2DESs). In particular, much of the experimental data on magnetotransport of electrons on the surface of liquid helium refer to range (1), with typical densities being $n \sim 10^8$ cm^{-2} (see Ref. 4). This range is also of interest for ultraclean low-density electron systems in semiconductors, which currently attract much attention.[5]

In range (1) all states within a broadened Landau level are nearly equally populated, and one no longer needs to take the Boltzmann factor into account while computing temperature and disorder averages using the Hamiltonian projected on that level. In spite of this simplification, we were unable to obtain an explicit solution of the problem. There are no good (nearly conserved) quantum numbers in the disorder-broadened band (such as quasimomentum, for example), and no small parameters characterize the intraband electron motion. However, as we show below, we can still accurately calculate the frequency-dependent conductivity. This is done by the method of moments, which was previously suggested for this problem by one of us.[6]

Our present analysis applies to a short-range disorder. For such disorder, the magnetotransport of noninteracting electrons in parameter range (1) was earlier analyzed[7,8] within the scope of the self-consistent Born approximation (SCBA). The SCBA ignores the interference effects which lead to

 ©2001 The American Physical Society

electron localization and the associated scaling behavior near the Landau band center. The uncontrolled nature of this approximation is especially evident in the static limit where the SCBA produces a nonzero conductivity, contrary to what is expected in the range (1) from the well-established IQHE theory where nearly all single-particle states are localized. From this point of view, it is important to develop a single-electron theory of magnetotransport that will take localization effects into account, and thus extend the ideas of the IQHE physics to a different parameter range.

Another motivation for developing such a theory comes from the experiment. A single-electron SCBA was used to interpret the data on the *static* magnetoconductivity of electrons on helium for strong enough magnetic fields[8–10] (for a review, see Refs. 11–13). Short-range disorder is a good model of the random potential in this system.[4] However, unless the variation of this potential in time is taken into account (this variation is *very* slow, both where the potential is due to ripplons or helium vapor atoms), the single-electron conductivity should be equal to zero, in contradiction with the observations. An important mechanism responsible for nonzero static conductivity is the electron-electron interaction. Our results reveal singular features of the single-electron conductivity, and also serve as a basis for the full many-electron theory of magnetoconductivity, which allows for strong electron-electron correlations.[14]

The outline of the paper is as follows. In Sec. II we calculate the frequency-dependent conductivity $\sigma_{xx}(\omega)$ in the temperature range $\hbar\gamma \ll k_BT$, $\exp(\hbar\omega_c/k_BT) \gg 1$ for $\omega \ll \omega_c$ (these results were previously announced in Ref. 14). We find the asymptotics of the conductivity at both small ($\omega \to 0$) and comparatively large ($\gamma \ll \omega \ll \omega_c$) frequencies, and show that $\sigma_{xx}(\omega)$ has a peak at a nonzero frequency $\omega \sim \gamma$. Using an efficient diagram classification scheme, we exactly compute the first 14 spectral moments of this peak. These moments contain information about the short-time ($\sim \gamma^{-1}$) dynamics of the system. Combined with the low- and high-frequency asymptotics, they allow us to accurately restore the entire function $\sigma_{xx}(\omega)$ (see Fig. 1). In Sec. III we investigate the cyclotron resonance, i.e., the dissipative conductivity for $\omega \approx \omega_c$. We calculate the first ten frequency moments of the cyclotron resonance absorption peak, and use them to accurately restore its shape (see Fig. 2) as a function of frequency detuning $\Delta\omega \equiv \omega - \omega_c$. To do the restoration, we also calculate the asymptotic form of the tails of the cyclotron resonance using the method of optimal fluctuation (our result differs from that obtained earlier by Ioffe and Larkin[15]). In Sec. IV we discuss the ways to observe the predicted here behavior in experiment. Technical details are given in the Appendixes.

II. LOW-FREQUENCY SINGLE-ELECTRON CONDUCTIVITY

In this section, we calculate the conductivity of a nondegenerate noninteracting two-dimensional electron system for low frequencies, $\omega \ll k_BT/\hbar$. We consider the case of a delta-correlated disorder potential, and assume that the broadening of the Landau level $\gamma \ll \omega_c, k_BT/\hbar$ [cf. Eq. (1)].

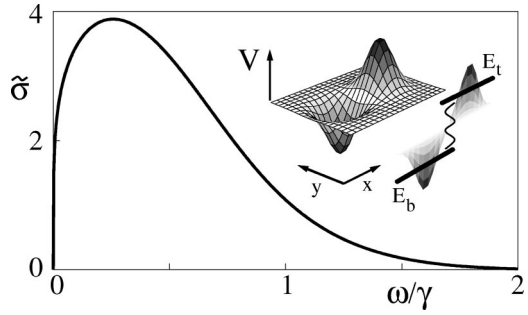

FIG. 1. Reduced microwave conductivity [Eq. (11)] of a noninteracting 2DES at the lowest Landau level in a short-range disorder potential for $\omega, \gamma \ll k_BT/\hbar$. For small frequencies $\omega \ll \gamma$, the conductivity is singular: $\sigma_{xx} \sim \omega^{\mu}$. It is determined by spatially large, nearly delocalized states. For $\omega \gg \gamma$, the conductivity is determined by large optimal fluctuations of the disorder potential, as illustrated in the inset. The optimal potential $V_{\rm opt}(\mathbf{r})$ is such that $\hbar\omega$ is equal to the energy difference $E_t - E_b$ between the top and bottom bound states $|t\rangle$ and $|b\rangle$, and at the same time these states are maximally overlapping.

In range (1) all states within the LLL are equally occupied, and the Kubo formula for the dissipative conductivity can be written as a simple trace without the Boltzmann factor:

$$\sigma_{xx}(\omega) = \frac{n(1-e^{-\beta\omega})}{\hbar\omega}\,\mathrm{Re}\int_0^\infty dt e^{i\omega t}\langle j_x(t)j_x(0)\rangle \qquad (2)$$

$$\approx \frac{n\beta}{2\hbar}\int_{-\infty}^{\infty} dt e^{i\omega t}\mathrm{Tr}_0\overline{\{j_x(t)j_x(0)\}}, \quad \beta\omega \ll 1. \qquad (3)$$

Here $j_x \equiv ep_x/m$ is the one-electron current operator, $\beta \equiv \hbar/k_BT$, the angular brackets $\langle\cdot\rangle$ denote statistical averaging over the states followed by an averaging over quenched disorder, and the horizontal line denotes only the disorder averaging. The trace Tr_0 in Eq. (3) is performed over all single-particle states of the lowest Landau level; the energies are measured with respect to its center. Equation (2) is written for the case of strongly quantizing magnetic fields,

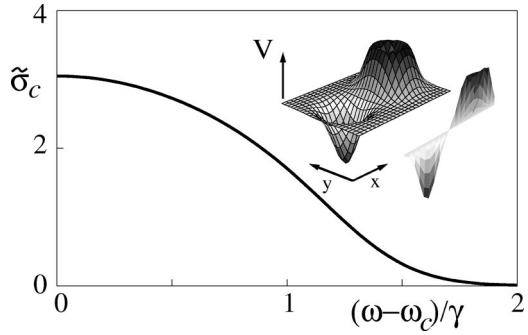

FIG. 2. Reduced conductivity at the cyclotron absorption peak [see Eq. (39)] of a noninteracting 2DES in a short-range disorder potential for $|\omega - \omega_c|, \gamma \ll k_BT/\hbar \ll \omega_c$. The curve is analytic in the center of the peak. The absorption at the tails, $|\omega - \omega_c| \gg \gamma$, is determined by large optimal fluctuations of the disorder potential, as illustrated in the inset.

$\exp(\beta\omega_c)\gg 1$, so that only the lowest Landau level is occupied. However, the calculation is readily generalized to the case of arbitrary $\beta\omega_c$ by replacing Tr_0 by the sum of traces over the states of each Landau level n, weighted with $\exp(-n\beta\omega_c)[1-\exp(-\beta\omega_c)]$.

Calculations within a single Landau level are conveniently done using the formalism of the guiding center coordinates $\mathbf{R}\equiv(X,Y)$. As explained in Appendix A, the electron dynamics in the random potential $V(\mathbf{r})$ is mapped onto that of a 1D quantum particle with the generalized momentum and coordinate X and Y, and with the Hamiltonian

$$H=\hbar\gamma\sum_{\mathbf{q}}\tilde{V}_{\mathbf{q}}\exp(i\mathbf{qR}),\quad [X,Y]=-il^2. \tag{4}$$

The guiding center velocity is determined by the potential gradient

$$\dot{R}_\mu=-il^2\gamma\sum_{\mathbf{q}}\epsilon_{\mu\nu}q_\nu\tilde{V}_{\mathbf{q}}e^{i\mathbf{qR}}, \tag{5}$$

where $\mu,\nu=x,y$, and $\epsilon_{\mu\nu}$ is the unit antisymmetric tensor: $\epsilon_{xy}=-\epsilon_{yx}=1$.

The dimensionless coefficients

$$\tilde{V}_{\mathbf{q}}\equiv(V_{\mathbf{q}}/\hbar\gamma)\exp(-l^2q^2/4) \tag{6}$$

are proportional to the Fourier components of the disorder potential,

$$V_{\mathbf{q}}\equiv S^{-1}\int d^2\mathbf{r}\,V(\mathbf{r})e^{-i\mathbf{qr}}, \tag{7}$$

where S is the area of the system. For higher Landau levels the coefficients $\tilde{V}_{\mathbf{q}}$ have to be modified as explained in Appendix A [see Eq. (A8)]. We will assume that $V(\mathbf{r})$ is zero-mean Gaussian and δ-correlated,

$$\overline{V(\mathbf{r})V(\mathbf{r}')}=v^2\delta(\mathbf{r}-\mathbf{r}'), \tag{8}$$

in which case the SCBA width of the lowest Landau band is[7] $\hbar\gamma=(2/\pi)^{1/2}v/l$.

In the simplified Kubo formula [Eq. (3)] the temperature dependence is factorized, and we can rewrite the low-frequency conductivity in the form of the generalized Einstein relation

$$\sigma_{xx}(\omega)=\frac{ne^2D}{k_BT}\frac{1}{8}\tilde{\sigma}(\omega), \tag{9}$$

where $D=l^2\gamma$ is the characteristic diffusion coefficient and, as discussed in Appendix A,

$$\tilde{\sigma}(\omega)\equiv\frac{2}{l^2\gamma}\int_{-\infty}^{\infty}dt\,e^{i\omega t}\mathrm{Tr}_0\{\overline{\dot{\mathbf{R}}(t)\cdot\dot{\mathbf{R}}(0)}\} \tag{10}$$

is the reduced conductivity. It depends on the ratio ω/γ of the only two quantities with the dimension of frequency that remain after projection on one Landau level.

Expression (10) can be rewritten, with the help of Eq. (5), as

$$\tilde{\sigma}(\omega)=-2l^2\gamma\int_{-\infty}^{\infty}dt\,e^{i\omega t}\sum_{\mathbf{q},\mathbf{q}'}(\mathbf{qq}')\times\mathrm{Tr}_0\{\overline{\tilde{V}_{\mathbf{q}}\tilde{V}_{\mathbf{q}'}\exp[i\mathbf{qR}(t)]\exp[i\mathbf{q}'\mathbf{R}(0)]}\}. \tag{11}$$

This form is particularly convenient for calculating the frequency moments of the reduced conductivity; see below in Sec. II C.

Yet another representation of the reduced low-frequency conductivity can be obtained if we describe time evolution of the electron operators in Eq. (11) using the set $|n\rangle$ of the eigenstates of the full electron Hamiltonian for the lowest Landau level, and perform the time integration

$$\tilde{\sigma}(\omega)=\frac{4\pi l^2}{\hbar\gamma}\sum_{n,m}\overline{\delta(E_n-E_m-\hbar\omega)|\langle n|\boldsymbol{\nabla}V|m\rangle|^2}, \tag{12}$$

where E_n are the energies of the LLL states $|n\rangle$ in the potential $V(\mathbf{r})$ (again, generalization to the case of several occupied Landau levels is straightforward).

We emphasize that, in the chosen parameter range, the Landau-level projection resulted in expressions that *do not* contain the usual disorder-dependent denominator, and the quenched disorder averaging can be done directly, without invoking supersymmetry or the replica trick. Nevertheless, the problem remains complicated as there are no good quantum numbers that would characterize the intraband electron motion.

A. Tail of the low-frequency conductivity

We begin by calculating the asymptotic form of the reduced conductivity $\tilde{\sigma}(\omega)$ for $\omega\gg\gamma$ from Eq. (12). In the neglect of interband mixing, the energies E_n are symmetrically distributed around the Landau band center ($E=0$). The tails of the density of states $\rho(E)$ are known to be Gaussian: $\rho(E)\propto\exp(-4E^2/\hbar^2\gamma^2)$. They are determined by the probability of the optimal (least improbable) potential fluctuation $V_E(\mathbf{r})$ in which the lowest or highest bound state has energy E ($|E|\gg\gamma$).[15,1,16]

If we ignore the matrix element in Eq. (12) altogether (as we show below, this only affects the prefactor), the tail of the conductivity will be proportional to the probability of finding two states E_n and E_m such that $E_n-E_m=\hbar\omega$. The major contribution comes from states at the opposite ends of the energy band with energies close to $E_n=-E_m=\hbar\omega/2$, giving

$$\tilde{\sigma}(\omega)\propto[\rho(\hbar\omega/2)]^2\propto\exp(-2\omega^2/\gamma^2). \tag{13}$$

To check this approximation, we will apply the method of optimal fluctuation.[17,15] The averaging over disorder in Eq. (12) will be done using the path-integral representation,

$$\overline{\mathcal{F}[V]}\equiv\int\mathcal{D}V(\mathbf{r})\mathcal{F}[V(\mathbf{r})]\exp\{-\mathcal{R}[V(\mathbf{r})]\}, \tag{14}$$

where, for a delta-correlated Gaussian potential with correlator (8),

$$\mathcal{R}[V]=\frac{1}{2v^2}\int d\mathbf{r}\,V^2(\mathbf{r}). \tag{15}$$

For large ω, the leading contribution to sum (12) comes from transitions between the states $|\psi_t\rangle$ and $|\psi_b\rangle$ with energies E_t and E_b at the top and bottom of the Landau band, respectively:

$$E_{t,b}=\int d\mathbf{r}\,V(\mathbf{r})|\psi_{t,b}(\mathbf{r})|^2. \tag{16}$$

To logarithmic accuracy, the conductivity is given by the solution of the variational problem of finding the optimal potential $V(\mathbf{r})$ which minimizes the functional $\mathcal{R}[V]$ and maximizes the matrix element of the transition subject to the constraint $E_t-E_b=\hbar\omega$, i.e.,

$$\tilde{\sigma}(\omega)\propto\max_V\{\exp[-\mathcal{R}[V]+\lambda(E_t-E_b-\hbar\omega)]\times|\langle\psi_t|\nabla V|\psi_b\rangle|^2\}, \tag{17}$$

where λ is a Lagrange multiplier. Variation with respect to $V(\mathbf{r})$ gives the equation

$$\frac{V(\mathbf{r})}{v^2}=\lambda(|\psi_t|^2-|\psi_b|^2)+\frac{\delta}{\delta V(\mathbf{r})}\ln|\langle\psi_t|\nabla V|\psi_b\rangle|^2 \tag{18}$$

(for brevity, we do not give the explicit form of the last term).

We have analyzed the variational problem using a simple and tractable direct variational method, and also by finding the maximum in Eq. (17) numerically. To see the qualitative features of the solution, we first discuss it ignoring the contribution of the matrix element. In this case the Lagrange multiplier λ is given by the consistency equation

$$\hbar\omega=E_t-E_b=v^2\lambda\int d\mathbf{r}(|\psi_t|^2-|\psi_b|^2)^2, \tag{19}$$

and then the conductivity [Eq. (17)] is

$$|\ln\tilde{\sigma}(\omega)|=\hbar^2\omega^2\left[2v^2\int d\mathbf{r}(|\psi_t|^2-|\psi_b|^2)^2\right]^{-1}. \tag{20}$$

Solution (18) corresponds to a potential of the form of a well and a hump, far away from each other (cf. Fig. 1). The potential is antisymmetric, and the well and the hump have the same Gaussian shape [$\propto\exp(-r^2/2l^2)$, with $\mathbf{r}$ counted off from the corresponding extremum] and opposite signs. The wave functions ψ_t and ψ_b are localized at the hump and the well of $V(\mathbf{r})$, respectively, and are given just by the most ''localized'' wave function of the lowest Landau level, namely, that with zero angular momentum, $\psi_{00}(\mathbf{r})\propto\exp(-r^2/4l^2)$, centered at the appropriate potential extremum. The overlap of these wave functions is negligibly small, and Eqs. (19) and (20) give

$$\hbar\omega=2v^2\lambda A,\quad |\ln\tilde{\sigma}(\omega)|=\frac{\hbar^2\omega^2}{4v^2A}=\frac{\omega^2}{2\pi\gamma^2l^2A},$$

with $A\equiv\int d\mathbf{r}|\psi_{t,b}|^4=(4\pi l^2)^{-1}$. In this way we recover expression (13) for the conductivity tail. For higher Landau levels ($N\gg1$), the wave functions have the form[16] $\psi_{t,b}\propto r^N\exp(-iN\phi)\exp(-r^2/4l^2)$, in which case the corresponding constant $A_N=(4\pi l^2)^{-1}(2N)!/2^{2N}(N!)^2$.

The prefactor in Eq. (17) prevents the well and hump of $V(\mathbf{r})$ from being too far away from each other. The full variational equation (18) has a solution with an antisymmetric optimal potential $V(\mathbf{r})=-V(-\mathbf{r})$ and symmetric wave functions $\psi_t(\mathbf{r})=\psi_b(-\mathbf{r})$: $E_t=-E_b=\hbar\omega/2$, respectively. To estimate the role of the overlap integral we used the direct variational method, in which we sought the potential in the form $V(\mathbf{r})=\tilde{V}(|\mathbf{r}-\mathbf{r}_0|)-\tilde{V}(|\mathbf{r}+\mathbf{r}_0|)$, with $\tilde{V}(r)=V_0\exp(-r^2/2l^2)$. The distance $2r_0$ separating the hump and the well was used as a variational parameter. Given the potential, one has to solve the Schrödinger equation, looking for the wave functions projected on the lowest Landau level. We took the functions $\psi_{t,b}$ in the simplest form of orthogonal combinations of the zero-momentum wave functions centered close to $\pm\mathbf{r}_0$ (the positions were found using a variational procedure). The distance r_0 scales logarithmically with frequency. The overall asymptotic expression for the exponent in $\tilde{\sigma}$ was the same as in Eq. (13); the overlap integral gave only a prefactor

$$|\langle\psi_t|\nabla V|\psi_b\rangle|^2\sim(\hbar\gamma^2/l\omega)^2\ln(\omega/\gamma).$$

[An extra ω-dependent contribution to the overall prefactor in $\tilde{\sigma}$ comes from the prefactor in path integral (14). It actually increases with the increasing ω. However, an evaluation of this prefactor goes beyond the scope of this paper, and in some sense is superseded by the results obtained below with the method of moments.]

To check the accuracy of the asymptotic behavior of $\tilde{\sigma}(\omega)$ further, we maximized[18] the functional in Eq. (17) numerically. We used the variational equation (18) to represent the optimal potential as a bilinear combination of the LLL wave functions $\psi_{0m}(\mathbf{r})\propto r^m\exp(im\phi)\exp(-r^2/4l^2)$ with different magnetic quantum numbers $m\geq0$:

$$V(\mathbf{r})=\sum_{m,m'}u_{mm'}\psi^*_{0m}(\mathbf{r})\psi_{0m'}(\mathbf{r}).$$

The corresponding eigenfunctions $\psi_{t,b}$ were written as linear combinations of the same functions $\psi_{0m}(\mathbf{r})$.

Both the exponent and prefactor of the variational functional (17) calculated numerically become close to the result of the direct variational method for $\omega/\gamma\gtrsim3$. The shape of the optimal potential found numerically for two values of ω/γ is illustrated in Fig. 3.

B. Conductivity at small frequencies

An entirely different set of states defines the conductivity for very small frequencies, $\omega\ll\gamma$. In this regime the constraint imposed by conservation of energy is not very restrictive, and it is the matrix element that determines relative contributions of different pairs of states. Close to the static limit the contribution to the conductivity increases dramati-

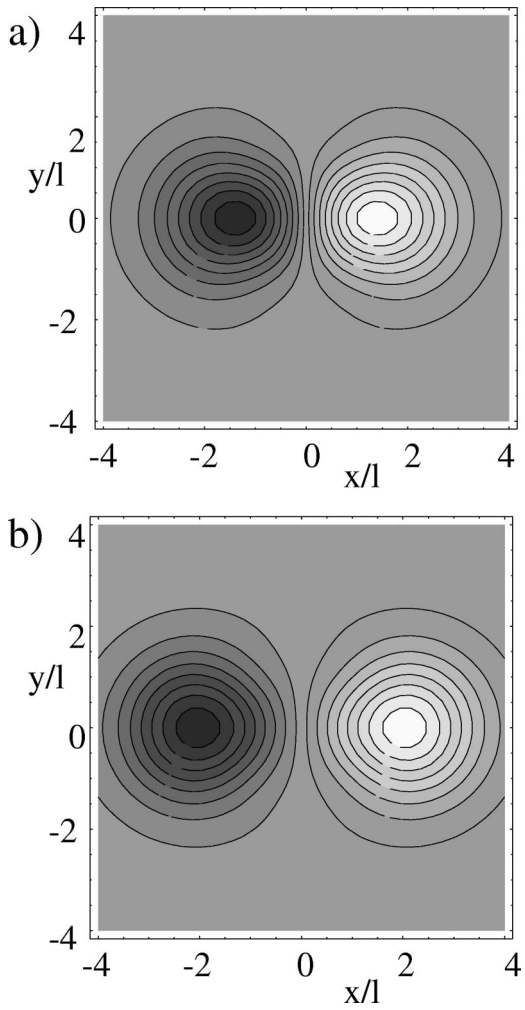

FIG. 3. Density plot of the optimal potential for $\omega=3\gamma$ (a) and $\omega=8\gamma$ (b). The distances are measured in units of the magnetic length l.

cally with the typical size of a wave function. As a result, $\tilde{\sigma}$ [Eq. (3)] is primarily determined by a narrow energy interval at the center of the Landau band where the states are nearly delocalized. The energy of the band center ($E=0$) is a critical energy, similar to the critical value of the control parameter in the theory of classical percolation transition. At small deviations from the critical energy (parametrized by dimensionless energy $\varepsilon\equiv E/\hbar\gamma$) the correlation length diverges, $\xi_\varepsilon\sim l|\varepsilon|^{-\nu}$, where $\nu=2.33\pm0.03$ is the localization exponent.[2,3,19]

Were it not for localization, propagation of a wave packet in a random potential would be diffusive:

$$\langle\Delta R^2(t)\rangle\sim Dt. \tag{21}$$

Localization corrections are least important near the critical energy, but even there they modify the form of a wave packet at very large times.[20] However, for not too large times the rms displacement retains a diffusive form. This can be used to find the conductivity at small frequencies.

To this end, let us rewrite Eq. (10),

$$\tilde{\sigma}(\omega)=-\frac{2\omega^2}{l^2\gamma}\lim_{\delta\to+0}\mathrm{Re}\int_0^\infty dt\, e^{i\omega t-\delta t}\mathrm{Tr}_0\overline{\Delta R^2(t)}, \tag{22}$$

in terms of the squared displacement $\Delta R^2(t)\equiv[\mathbf{R}(t)-\mathbf{R}(0)]^2$, where $\mathbf{R}(t)\equiv e^{iHt}\mathbf{R}\,e^{-iHt}$ is the Heisenberg operator of the guiding center. For an eigenstate $|n\rangle$ of Hamiltonian (4) randomly chosen not too far from the critical energy, $\langle n|\Delta R^2(t)|n\rangle$ has a diffusive form [Eq. (21)] at small enough t, but it eventually saturates at the distance of the order of the localization length ξ_{ε_n}. Replacing the trace by the integral over energy weighted with the (noncritical) density of states, we obtain the overall long-time ($\gamma t\gg1$) rms displacement

$$\mathrm{Tr}_0\overline{\Delta R^2(t)}\sim\hbar\gamma\int d\varepsilon\,\rho(\hbar\gamma\varepsilon)\min(Dt,\xi_\varepsilon^2)\propto l^2(\gamma t)^{1-1/(2\nu)}. \tag{23}$$

This average is determined by the states with energies $|\varepsilon|\lesssim(\gamma t)^{-1/2\nu}$; the integral rapidly converges outside this region.

With asymptote (23), time integration in Eq. (22) gives

$$\tilde{\sigma}(\omega)=C(\omega/\gamma)^\mu,\quad \mu\equiv(2\nu)^{-1}. \tag{24}$$

The same result can be obtained from the scaling form[21,22] of the zero-temperature conductivity of the noninteracting system at a given chemical potential, which can be written as

$$\sigma_{xx}(\varepsilon,\omega)=\frac{e^2}{\hbar}\mathcal{G}_0\left(\frac{\omega\xi_\varepsilon^2}{\gamma l^2}\right), \tag{25}$$

where the dimensionless scaling function $\mathcal{G}_0(X)$ rapidly vanishes for $X\to0$, and approaches a constant value for large X. Indeed, the conductivity for $\beta\omega\ll1$ can be written as a convolution of scaling function (25), with the derivative of the Fermi distribution function

$$\tilde{\sigma}(\omega)=\frac{8k_BT}{ne^2l^2\gamma}\int d\varepsilon\left(-\frac{dn_F}{d\varepsilon}\right)\sigma_{xx}(\varepsilon,\omega) \tag{26}$$

[cf. Eq. (9)]. For $k_BT\gg\hbar\gamma$, all energies within the stripe of width $\delta\varepsilon\sim(\omega/\gamma)^\mu$ contribute equally, and in the limit $\omega\to0$ we obtain Eq. (24), with the coefficient

$$C=16\pi\mu\int_{-\infty}^{\infty}\frac{dX}{|X|^{1+\mu}}\tilde{\mathcal{G}}_0(X). \tag{27}$$

Here we have assumed that $\varepsilon^\nu\xi_\varepsilon\to\mathrm{const}$ for $\varepsilon\to0$, and $\tilde{\mathcal{G}}_0(X)\equiv\lim_{\varepsilon\to0}\mathcal{G}_0(X\varepsilon^{2\nu}\xi_\varepsilon^2/l^2)$. The integration converges both at zero and infinity.

C. Spectral moments

Since the single-particle conductivity goes to zero both for $\omega\to0$ and for $\omega\gg\gamma$, its frequency dependence displays a peak, with a maximum at a nonzero frequency $\omega\sim\gamma$. Such a peak is of central interest from the point of view of experiment; it does not occur in the SCBA. This peak was found and briefly discussed in our previous paper.[14] Here we

present the results and provide some details of the full calculation of the low-frequency conductivity based on the method of spectral moments. The advantageous feature of this method is that, instead of solving the full time-dependent problem of the electron motion in a random field [Eq. (5)], one has to evaluate only equal-time correlation functions.

We first calculate the spectral moments of the reduced conductivity $\tilde{\sigma}(\omega)$ [Eq. (9)]. They are defined as

$$M_k=\frac{1}{2\pi\gamma}\int_{-\infty}^{\infty}d\omega(\omega/\gamma)^k\tilde{\sigma}(\omega). \tag{28}$$

For $\omega,\gamma\ll k_BT/\hbar$, the states within the broadened Landau level are equally populated, and the conductivity is an even function of frequency, $\tilde{\sigma}(\omega)=\tilde{\sigma}(-\omega)$. Therefore all odd moments vanish, $M_{2k+1}=0$. For even moments, we use Hamiltonian (4) to obtain from Eqs. (11) and (28):

$$M_{2k}=-2l^2\sum(\mathbf{q}_1\mathbf{q}_{2k+2})\overline{\tilde{V}_{\mathbf{q}_1}\cdots\tilde{V}_{\mathbf{q}_{2k+2}}} \times[[\cdots[e^{i\mathbf{q}_1\mathbf{R}},e^{i\mathbf{q}_2\mathbf{R}}],\ldots],e^{i\mathbf{q}_{2k+1}\mathbf{R}}]e^{i\mathbf{q}_{2k+2}\mathbf{R}}. \tag{29}$$

The summation is performed over all $\mathbf{q}_1,\ldots,\mathbf{q}_{2k+2}$. Commutator (29) can be evaluated recursively using

$$[e^{i\mathbf{q}\mathbf{R}},e^{i\mathbf{q}'\mathbf{R}}]=2i\sin\left(\frac{1}{2}l^2\mathbf{q}\wedge\mathbf{q}'\right)e^{i(\mathbf{q}+\mathbf{q}')\mathbf{R}}. \tag{30}$$

For Gaussian random potential, the disorder average in Eq. (29) can be computed by Wick's theorem. From Eqs. (6)–(8)

$$\langle\tilde{V}_{\mathbf{q}}\tilde{V}_{\mathbf{q}'}\rangle=(\pi l^2/2S)\exp(-l^2q^2/2)\delta_{\mathbf{q}+\mathbf{q}',\mathbf{0}},$$

where S is the area of the system. Then

$$M_{2k}=-\pi\left(-\frac{l^2}{2\pi}\right)^{k+2}\sum_{\mathcal{C}(\{\mathbf{q}\})}\int d\mathbf{q}_1\cdots d\mathbf{q}_{2k+2}\mathcal{C}(\{\mathbf{q}\}) \times(\mathbf{q}_1\mathbf{q}_{2k+2})\exp\left(-\frac{l^2}{4}(q_1^2+\cdots+q_{2k+2}^2)\right) \times\sin\left(\frac{l^2}{2}\mathbf{q}_1\wedge\mathbf{q}_2\right)\sin\left(\frac{l^2}{2}(\mathbf{q}_1+\mathbf{q}_2)\wedge\mathbf{q}_3\right)\cdots \times\sin\left(\frac{l^2}{2}(\mathbf{q}_1+\mathbf{q}_2+\cdots+\mathbf{q}_{2k})\wedge\mathbf{q}_{2k+1}\right), \tag{31}$$

where the sum is taken over all $(2k+1)!!$ ways to choose pairs out of the set of $2k+2$ variables, and

$$\mathcal{C}(\{\mathbf{q}\})\equiv\delta(\mathbf{q}_{i_1}+\mathbf{q}_{j_1})\cdots\delta(\mathbf{q}_{i_{k+1}}+\mathbf{q}_{j_{k+1}})$$

is the corresponding *contraction* function.

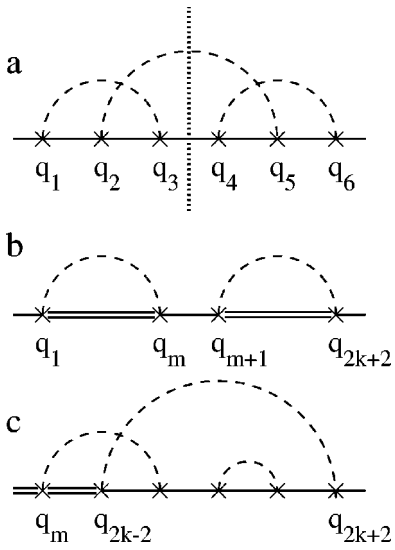

FIG. 4. Examples of diagrams. Dashed lines indicate which variables are paired, and double lines represent an arbitrary internal structure. (a) A symmetric diagram. Diagrams whose contribution is equal to zero: (b) *disconnected* diagrams, and (c) diagrams which vanish because the associated function is odd in $\mathbf{q}_{2k+2}$.

To classify different terms in sum (31), it is convenient to depict the contraction procedure graphically as illustrated in Fig. 4. (These diagrams merely represent the contraction function $\mathcal{C}$ and should not be confused with Feynman diagrams for the Green's functions.) First we note that the sequence of $\mathbf{q}_i$, paired in a diagram, may be reversed, $\mathbf{q}_i\rightarrow\mathbf{q}_{2k+3-i}$, without changing the overall value of the diagram. The diagrams obtained by such a reversal are equivalent, which reduces the computation cost by a factor of two [this reduction does not occur, however, for symmetric diagrams shown in Fig. 4(a)]. An additional simplification comes from the fact that disconnected diagrams [Fig. 4(b)] and the diagrams with the structure shown in Fig. 4(c) are equal to zero. The number of diagrams of different sorts is given in Ref. 18; for example, for the 14th moment there are 2027035 diagrams, out of which 5937 are symmetric, and 318631 are disconnected; the contribution of the diagrams with $\mathbf{q}_1=-\mathbf{q}_2$ is ≈ 72.559, whereas the contribution of all other diagrams is ≈ -8.809.

Despite the reductions, the number of terms to be calculated remains very large for large k. Moreover, each term in Eq. (31) is a sum of 2^{2k} Gaussian integrals. Each integral can be calculated algebraically but at a high computational cost. To accelerate the calculation, we have devised an efficient numeric classification scheme, which sorts diagrams inexpensively into *bins* according to their approximate values calculated with double precision. A representative diagram is evaluated algebraically for each bin. Finally, the diagrams are summed up with proper multiplicity, giving *exact* numerical values of the moments. The procedure is outlined in Appendix B. Algebraically calculating only nonequivalent Gaussian integrals reduces the computational time tremendously. This allowed us to evaluate the moments up to M_{14}. For $k=0,1,\ldots,7$, we obtain

$$M_{2k}=1,\frac{3}{8},\frac{443}{1152},\frac{25003}{38400},\frac{13608949709}{8941363200},\frac{298681273551508807}{66698308912435200},\frac{566602308094143977186611746328323669809}{3603336445266928972675556730863616000},$$

$$\frac{258900891167704930828461705265328752472466933109337279241227045993970 1}{406119740082234236083813556172406663141442907874062935031860428800 00},\tag{32}$$

and the corresponding approximate values

$$M_{2k}\approx 1,0.375,0.385,0.651,1.522,4.478,15.72,63.75.$$

D. Reconstruction of frequency dependence

Since the conductivity is asymptotically Gaussian, one is tempted to restore $\tilde{\sigma}(\omega)$ from the moments M_n in a standard way, writing an expansion in Hermite polynomials $\tilde{\sigma}(\gamma x)=\Sigma_n B_n H_n(\sqrt{2}x)\exp(-2x^2)$. The coefficients B_n can be expressed recursively in terms of the moments M_k, $k\leqslant n$. However, for moments (32), this expansion does not converge rapidly; see Fig. 5. This is consistent with *nonanalyticity* of the conductivity at $\omega=0$.

Given the exponent μ in Eq. (24), a much more rapidly convergent expansion can be constructed in terms of a different set of orthogonal polynomials. Specifically, with Eqs. (13) and (24), we write the conductivity at the lowest Landau level as

$$\tilde{\sigma}(\omega)=x^{\mu}G(x)\exp(-2x^2),\quad x\equiv|\omega|/\gamma.\tag{33}$$

The function $G(x)$ $(x\geqslant 0)$ can be expanded in Laguerre polynomials $L_n^{(\mu-1)/2}(2x^2)$, which are orthogonal for the weighting factor in Eq. (33). It is important that the expansion coefficients can also be recursively restored from the moments M_{2k}, $k\leqslant n$.

For the presently accepted value of the localization exponent $\nu\approx 2.33$, the value of the conductivity exponent μ is 0.215. The expansion for G converges rapidly for μ between 0.19 and 0.28, whereas outside this region the convergence deteriorates, as illustrated in Fig. 6. This could be considered as an indirect indication of the consistency of our approach.

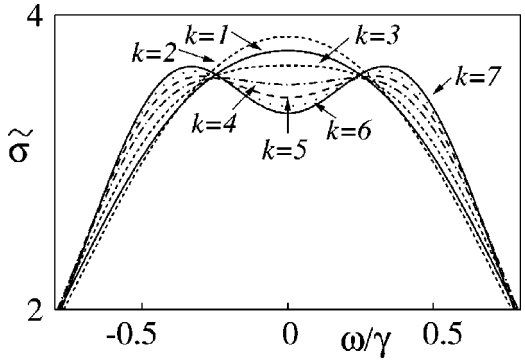

FIG. 5. Approximating $\tilde{\sigma}(\omega)$ with Hermite polynomials. With an increasing number of moments M_{2k}, a minimum of the conductivity develops, consistently at $\omega=0$, and the expansion does not show a fast convergence for small ω/γ.

The resulting conductivity calculated with $\mu=0.215$ is shown in Fig. 1. The estimated deviation from the obtained curve, due to the finite number of moments and also to the uncertainty in the value of μ (its effect is discussed in Ref. 18), is smaller than the width of the line.

III. SINGLE-ELECTRON CYCLOTRON RESONANCE

Resonant single-electron absorption near the cyclotron frequency $(\omega\approx\omega_c)$ is determined by the correlation function of the Landau-level raising and lowering operators $p_{\pm}$ defined in Appendix A,

$$\sigma_c(\omega)=\frac{ne^2}{2m}\int_{-\infty}^{\infty}dt\,e^{i\omega t}\langle p_-(t)p_+(0)\rangle,\tag{34}$$

where we used Eq. (2), assuming $\exp(\hbar\omega_c/k_BT)\gg 1$, in which case only the lowest Landau level is occupied for small densities. In fact, Eq. (34) gives not only the real part of the diagonal conductivity $\sigma_{xx}(\omega)$, but also the dissipative part of the off-diagonal components of the conductivity tensor,

$$\mathrm{Im}\,\sigma_{xy}(\omega)=-\,\mathrm{Im}\,\sigma_{yx}(\omega)\approx\mathrm{Re}\,\sigma_{xx}(\omega),\tag{35}$$

for $\omega\approx\omega_c$. Therefore it determines resonant absorption of both linearly and circularly polarized light.

Relation (35) implies strong circular dichroism. In the absence of disorder, because of the selection rule associated

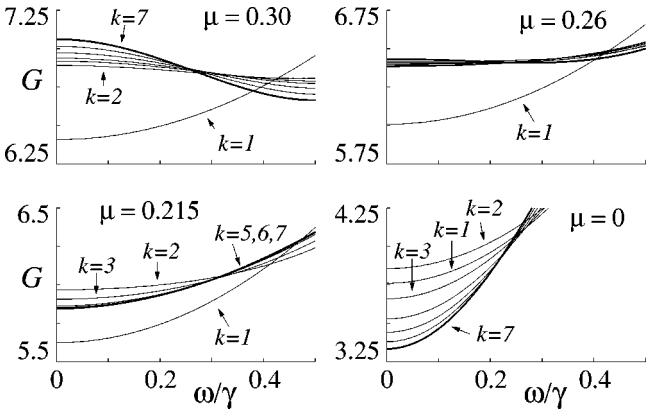

FIG. 6. The expansion of the prefactor G [Eq. (33)] in Laguerre polynomials $L_n^{(\mu-1)/2}(2x^2)$ for different values of the exponent μ, depending on the total number of moments M_{2k}. The expansion converges rapidly for μ between 0.19 and 0.28, and much more slowly outside this interval.

with the angular momentum conservation, only one circularly polarized component is absorbed. Disorder potential breaks the symmetry, and leads to a violation of the selection rule. However, for weak disorder this violation is weak. An analysis analogous to that in Appendix A shows that the absorption coefficient for the ''forbidden'' polarization is proportional to that of the strongly absorbed one, as given by Eqs. (34) and (35), but contains an extra frequency-dependent factor of order γ^2/ω_c^2.

If the disorder is weak, $\gamma \ll \omega_c$, it only weakly mixes different Landau levels, the primary effect being to lift the degeneracy of each level. Then the problem of optically induced transitions between different Landau levels resembles that of transitions between degenerate electronic terms of impurities in solids in the presence of the electron-phonon coupling, which gives rise to the Jahn-Teller effect.[23] One of the effective methods of the theory of absorption spectra of Jahn-Teller centers is the method of moments (MOM).

The MOM formalism can be transferred to the case of inter-Landau-level transitions. For $\hbar\gamma \ll k_B T$, quenched disorder can be described in the same way as scattering by thermally excited phonons. However, in the case of 2DES one should allow for infinite level degeneracy.

In the neglect of disorder-induced scattering between Landau levels, one should keep only the part H_d of the disorder potential $V(\mathbf{r})$, which is diagonal in the Landau-level representation,

$$H_d = \sum_N H_d^{(N)} P_N = \hbar\gamma \sum_{\mathbf{q}} \tilde{V}_{\mathbf{q}} e^{i\mathbf{qR}} \sum_N L_N\left(\frac{q^2 l^2}{2}\right) P_N, \tag{36}$$

where $\tilde{V}_{\mathbf{q}}$ is defined by Eq. (6) and $P_N = P_N^2$ is the operator of projection to the Nth Landau level, as in Eq. (A7). With Hamiltonian (36), oscillations at the cyclotron frequency can be singled out in Eq. (34),

$$p_{\pm}(t) = e^{\pm i\omega_c t} e^{iH_d t/\hbar} p_{\pm} e^{-iH_d t/\hbar}. \tag{37}$$

Then, from Eq. (34), we can write

$$\sigma_c(\omega) = \frac{ne^2}{2m\gamma} \tilde{\sigma}_c(\omega), \tag{38}$$

where

$$\tilde{\sigma}_c(\omega) = \gamma \int_{-\infty}^{\infty} dt\, e^{i\Delta\omega t} \mathrm{Tr}_0 \overline{[e^{iH_d t/\hbar} p_- e^{-iH_d t/\hbar} p_+]} \tag{39}$$

is the reduced conductivity, and $\Delta\omega \equiv \omega - \omega_c$ is the frequency detuning, $|\Delta\omega| \ll \omega_c$.

The major difference of Eq. (39) from its low-frequency counterpart [Eq. (10)] is that the Hamiltonians for direct and inverse time propagation (corresponding to the factors $e^{\pm iH_d t}$) are now different, which is again familiar from the theory of impurity absorption spectra. The reduced cyclotron conductivity can be conveniently written in a form conventional for this theory by introducing the ''perturbation'' Hamiltonian:

$$\delta H_d \equiv H_d^{(1)} - H_d^{(0)} = -\hbar\gamma \sum_{\mathbf{q}} \frac{q^2 l^2}{2} \tilde{V}_{\mathbf{q}} e^{i\mathbf{qR}}. \tag{40}$$

In the interaction representation, $\tilde{\sigma}_c$ can be then expressed in terms of a time-ordered exponential:

$$\tilde{\sigma}_c(\omega) = \gamma \int_{-\infty}^{\infty} dt\, e^{i\Delta\omega t} \mathrm{Tr}_0 \left[\overline{\mathrm{T}_\tau \exp\left(-\frac{i}{\hbar} \int_0^t d\tau\, \delta H_d(\tau) \right)} \right]. \tag{41}$$

Here the time dependence of the operator δH_d,

$$\delta H_d(\tau) \equiv e^{iH\tau/\hbar}\, \delta H_d\, e^{-iH\tau/\hbar}, \quad H \equiv H_d^{(0)}, \tag{42}$$

is generated by the disorder Hamiltonian projected on the LLL, which is given by Eq. (4) of Sec. II.

We can now define the spectral moments of the cyclotron peak as

$$M_k^c = \frac{1}{2\pi\gamma} \int_{-\infty}^{\infty} d\omega \left(\frac{\omega - \omega_c}{\gamma}\right)^k \tilde{\sigma}_c(\omega). \tag{43}$$

Using Eq. (41) we write

$$M_k^c = \mathrm{Tr}_0 \overline{\left(\frac{i}{\gamma}\frac{d}{dt}\right)^k \mathrm{T}_\tau \exp\left(-\frac{i}{\hbar} \int_0^t \delta H_d(\tau) d\tau \right)} \Bigg|_{t=0}. \tag{44}$$

We note that, similar to the case of the peak of low-frequency conductivity discussed in Sec. II, here we calculate the moments of the cyclotron peak only, whereas the small ($\propto \gamma^2/\omega_c^2$) correction from the correlators neglected in obtaining Eq. (34) is projected away, as are the peaks of $\sigma_{xx}(\omega)$ at $\omega \approx n\omega_c$ with $n \neq 1$.

A. Tails of the cyclotron resonance peak

As in Sec. II let us first discuss the asymptotic form of the cyclotron peak comparatively far from resonance, $|\Delta\omega| \gg \gamma$ (yet $|\Delta\omega| \ll \omega_c$). If we introduce the exact eigenstates of Hamiltonian (36) for the lowest $|0,m\rangle$ and first excited $|1,m\rangle$ Landau levels, with energies $E_m^{(0)}$ and $E_m^{(1)}$, respectively, expression (39) for the reduced conductivity can be written in the form

$$\tilde{\sigma}_c(\omega) = 2\pi\hbar\gamma \sum_{m,n} \overline{\delta(E_m^{(1)} - E_n^{(0)} - \hbar\omega) |\langle 1,m|p_+|0,n\rangle|^2}. \tag{45}$$

As for the low-frequency conductivity considered in Sec. II, the conductivity tail is determined by large optimal fluctuations of the disorder potential.

The problem of the optimal potential for cyclotron resonance was previously considered by Ioffe and Larkin.[15] They used an ansatz of a rotationally symmetric optimal potential

$$V_{\mathrm{opt}}^{\mathrm{IL}} = 2\pi V_0 |\Phi_0|^2 + 2\pi V_1 |\Phi_1|^2, \tag{46}$$

where $\Phi_0 = \psi_{0,0}(\mathbf{r})$ and $\Phi_1 = \psi_{1,-1}(\mathbf{r})$ are the functions of the lowest and first excited Landau levels centered at the *same* origin, with magnetic quantum numbers 0 and -1,

respectively. This resulted in the asymptotic form of the cyclotron resonance absorption peak $\sigma_c \propto \exp(-8\Delta\omega^2/\gamma^2)$ for the range $\hbar\gamma \ll k_B T$.

We argue that the transition probability between the states with energy separation $E_m^{(1)} - E_n^{(0)} = \Delta\omega + \omega_c$ is exponentially increased if the cyclotron orbit centers of these states are permitted to shift with respect to each other. This happens despite the associated decrease of the overlap integral.

The calculation of the tails of the cyclotron resonance absorption peak is very similar to that in Sec. II A. We begin by writing the averaging in terms of a functional integral [Eq. (14)], with the energy conservation taken into account using a Lagrange multiplier [as in Eq. (17), but with *different* Hamiltonians for E_t and E_b]. If we neglect the dependence of the transition matrix element on $V(\mathbf{r})$, then for the optimal potential we obtain an equation similar to Eq. (46). However, in contrast to Ref. 15, we permit the centers of the wave functions Φ_0 and Φ_1 to be shifted with respect to each other. A remarkable feature of this simplified variational problem is that, in the neglect of overlapping of the displaced wave functions, the *same* value of the variational functional (except for the overlap term) is obtained for the trial wave functions of the first Landau level with the magnetic quantum numbers -1 or 0, i.e., $\psi_{1,-1}$ or $\psi_{1,0}$, or for any their linear combination.

For a displacement R between the centers of the hump and well of the optimal potential, the transition matrix element is $|\langle \psi_1 | p_+ | \psi_0 \rangle| \sim \exp(-R^2/4l^2)$. The optimal distance $R^2 \approx 4l^2 \ln[(\omega-\omega_c)^2/\gamma^2]$ is found by maximizing the expression with the matrix element present. As in the case of the low-frequency conductivity, this distance increases as the frequency is tuned away from resonance.

The variational result for the conductivity tail is

$$\tilde{\sigma}_c(\omega) \propto \exp\left(-\frac{8}{3\gamma^2}(\omega-\omega_c)^2 \right). \tag{47}$$

This tail is much broader, with the exponent reduced by a factor of 3, compared to the result of Ref. 15.

B. Center of the cyclotron absorption peak

Generally, we do not expect $\tilde{\sigma}_c(\omega)$ to display a nonanalytic dip at the center of the cyclotron absorption peak. Indeed, the power-law singularity [Eq. (24)] of the low-frequency conductivity can be associated with quantum interference, which leads to an eventual localization of all states except for one (or maybe a few) at the band center. Expression (41) for the cyclotron resonance absorption has a structure which differs from that for the low-frequency conductivity. In particular, it contains an extra phase factor from the Hamiltonian δH_d [Eq. (40)] which represents the difference in the random potential experienced by an electron at the two Landau levels. This phase factor should give rise to an exponential damping, and related suppression of the interference effects at long times. Consequently, the conductivity is expected to be smooth near ω_c.

Another way to see this is based on the following arguments. The suppression of the low-frequency conductivity for $\omega \to 0$ may be attributed to level repulsion between overlapping localized states. This repulsion is comparatively small for states of relatively large radii, with energies close to the band center. Indeed, only such states contribute to the low-frequency conductivity, as we saw in Sec. II B. On the other hand, resonant cyclotron absorption is due to transitions between *different* Landau levels. Although the central part of the absorption peak is formed by transitions between strongly overlapping states, the involved states are eigenstates of *different* Hamiltonians, with random parts $H_d^{(0)}$ and $H_d^{(1)}$. Their wave functions have different spatial structures, and their energies are essentially uncorrelated, except for states deep in the tails of the Landau levels. Consequently, we expect no suppression of transitions at frequencies close to ω_c. This argument is in agreement with the results of the method of moments presented in Sec. III C and Fig. 2.

C. Spectral moments of the cyclotron peak

We will now calculate the spectral moments [Eq. (44)]. Because all states of the lowest Landau level are equally populated, the reduced conductivity [Eq. (41)] is symmetric with respect to ω_c, i.e., $\tilde{\sigma}_c(\omega_c+\Delta\omega) = \tilde{\sigma}_c(\omega_c-\Delta\omega)$. Therefore, all odd moments vanish, $M_{2k+1}^c = 0$. The structure of the expression for even moments which follows from Eq. (44) is similar to that of Eq. (31). The main difference is that the prefactor is now a complicated polynomial, a combination of products of terms which are linear in the squared wave numbers q_k^2.

This strongly complicated the numerical procedure. In particular, we failed to find any symmetries to reduce the computational overhead, and graphical representations were of little help. We were also unable to categorize different terms as described in Appendix B for the low-frequency conductivity. Instead, we developed the computer algebra package GaussInt (Ref. 24) for Mathematica, capable of handling the integration of high dimensional Gaussian integrals in a manageable time frame, and used the brute-force approach calculating all terms analytically. For $k = 0,1,\ldots,5$ we obtained

$$M_{2k}^c = 1; \frac{1}{2}, \frac{37}{64}, \frac{52043}{55296}, \frac{4750893001499}{2488320000000}, \frac{296940541883532752078319507164960546 87}{64806963339141176117211168768000000000}, \tag{48}$$

and the corresponding approximate values

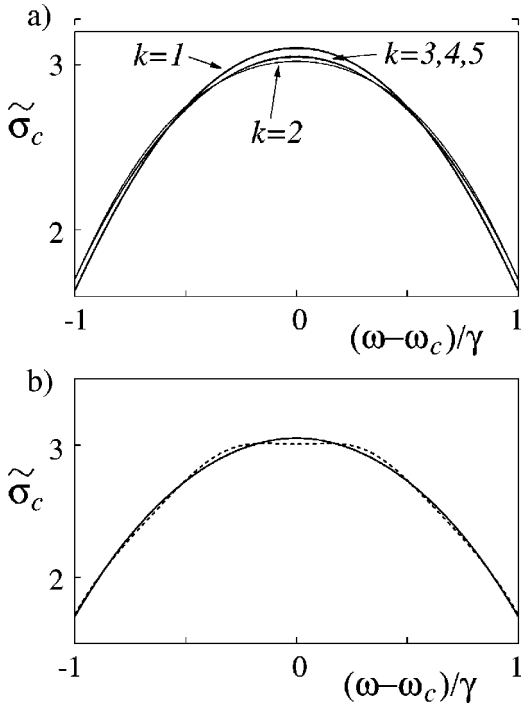

FIG. 7. Approximating $\tilde{\sigma}_c$ with continued fractions. (a) The convergence with increasing number of moments M_{2k}^c is extremely fast: the curves lie on top of each other already for $k=3,4$, and 5. (b) A comparison between the continued fraction (solid line) and the Hermite polynomial approximation (dashed line) for $k=5$. Convergence is much faster with continued fractions.

$$M_{2k}^c \approx 1.000, 0.500, 0.578, 0.941, 1.909, 4.582.$$

The values of the moments with $k=0,1$, and 2 were also independently confirmed analytically.

D. Reconstruction of frequency-dependence

As a first step, we reconstructed $\tilde{\sigma}_c(\omega)$ using a standard expansion in Hermite polynomials:

$$\tilde{\sigma}_c(\gamma x) = \sum_n B_n H_n(\sqrt{8/3}x)\exp(-8x^2/3).$$

The coefficients B_n were expressed recursively from the calculated moments [Eq. (48)]. We discovered that although the convergence is fast far from the center of the peak, it is noticeably slower close to the center (we emphasize, however, that we reached convergence, in contrast to the similar expansion for the low-frequency conductivity in Fig. 5, where the convergence was not reached for 14 moments). Within this approach, the number of calculated moments is apparently insufficient for restoring the entire function $\tilde{\sigma}_c$ with desired accuracy. The corresponding result is shown by the dashed line in Fig. 7.

Much faster convergence was achieved when $\tilde{\sigma}_c(\omega)$ was restored using a continued fraction expansion. We applied an algorithm similar to that used to reconstruct the LLL density of states from its frequency moments for an arbitrary correlated random potential.[25] The steps involved in this process are summarized in Appendix C. As one can see from Fig. 7, the convergence is very fast. The resulting shape of the cyclotron absorption peak is shown in Fig. 2. We believe that the deviation from the exact value is within the width of the curve.

IV. CONCLUSION

In conclusion, we have analyzed the single-electron low-frequency magnetoconductivity and cyclotron resonance absorption of a nondegenerate 2D electron system in a quantizing magnetic field. We considered the experimentally important parameter range where the width of the Landau levels is less than temperature, so that all states within the lowest Landau level are equally populated. In this range, by combining the ideas of the scaling theory of the IQHE, the method of optimal fluctuation, and the method of spectral moments, we obtained highly accurate numerical results throughout the frequency domain where the conductivity displays peaks.

We found that, in contrast to the prediction of the SCBA or other mean-field theories,[26] the low-frequency conductivity displays a peak at a *nonzero* frequency, as shown in Fig. 1. For short-range disorder, the position of the peak is given by

$$\omega_m \approx 0.26\gamma. \tag{49}$$

For $\omega \to 0$, the single-electron conductivity displays a *universal* power-law dispersion $\sigma_{xx} \propto \omega^{\mu}$, which is related to the scaling behavior of the localization length as a function of the distance in energy from the center of the disorder-broadened Landau level. On the other hand, the peak of the cyclotron resonance does not display such singular behavior, and is not shifted away from ω_c, as seen from Fig. 2. Both peaks have Gaussian tails, with different exponents [see Eqs. (13), (47)].

Experimentally, it may be more feasible to investigate the magnetoconductivity at a given nonzero frequency ω as a function of the external magnetic field B. The corresponding representation of our results is given in Fig. 8 for the scaled conductivity $\sigma_*(B;\omega)$,

$$\sigma_* \equiv \sigma_*(B;\omega) = \left[\frac{B_0(\omega)}{B}\right]^{1/2} \frac{\tilde{\sigma}(\omega)}{\tilde{\sigma}(\gamma)}, \tag{50}$$

where the scaling factor is $\tilde{\sigma}(\gamma) \approx 1.08$. The scaling field $B_0(\omega)$ is defined by the equation $\gamma=\omega$ for $B=B_0$, which gives $B_0(\omega) = \pi m c \tau_0 \omega^2/2|e|$, where $\tau_0^{-1} = v^2 m/\hbar^3$ is the rate of electron scattering by the short-range potential [Eq. (8)] in the absence of the magnetic field.

The magnetoconductivity σ_{xx} is related to $\sigma_*(B;\omega)$ by a factor which is independent of B but depends on ω:

$$\sigma_{xx}(\omega) = \frac{\tilde{\sigma}(\gamma)}{4\pi} \frac{\hbar}{k_B T} \frac{ne^2}{m\omega\tau_0} \sigma_*(B;\omega). \tag{51}$$

In the self-consistent Born approximation, the function $\sigma_*(B;\omega)$ decays with the increasing magnetic field as $B^{-1/2}$, for $B \gg B_0(\omega)$. With the localization effects taken into ac-

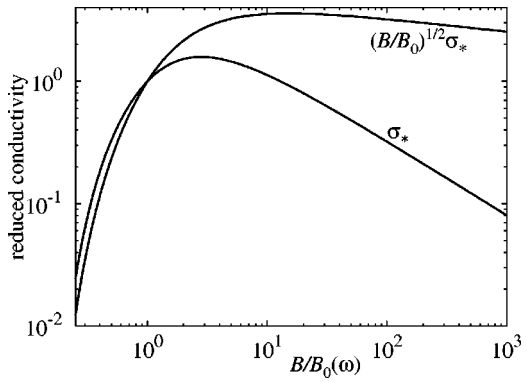

FIG. 8. Reduced ac magnetoconductivity σ_* [Eq. (50)] at a nonzero frequency ω as a function of the reduced magnetic field $B/B_0(\omega) \propto B\,\omega^{-2}$. In order to demonstrate the anomalous single-electron behavior, σ_* is also plotted with an extra factor $(B/B_0)^{1/2}$. For large B, the single-electron conductivity displays a scaling behavior: $B^{1/2}\sigma_* \propto B^{-\mu/2}$.

count, this dependence becomes steeper, with $B^{1/2}\sigma_* \propto B^{-\mu/2}$, as illustrated in Fig. 8.

Within the single-electron approximation, the restriction on the magnetic field from above is imposed by the condition $\hbar\gamma \ll k_B T$, which is equivalent to $\omega_c \ll \tau_0 (k_B T/\hbar)^2$ for the short-range disorder potential. This inequality can be fulfilled simultaneously with $B \gg B_0(\omega)$, provided $\hbar\omega \ll k_B T$. The restriction on the magnetic field from below, necessary for the system to be in the lowest Landau level, $\hbar\omega_c \gg k_B T$, can hold for $B \sim B_0(\omega)$ and $\hbar\omega \ll k_B T$, provided $k_B T \gg \hbar\tau_0^{-1}$.

The latter inequality is often fulfilled for electrons on a helium surface. This system displays the highest electron mobilities observed in condensed-matter systems. We believe that it is important to reconcile the experimental data on the magnetoconductivity of electrons on helium with the theory of the integer quantum Hall effect.

For $T < 0.9$ K the random potential experienced by electrons on helium is due mostly to capillary waves, ripplons. It has a small correlation length and is quasistatic. For electron densities $n \sim 10^8$ cm^{-2} and $T = 0.7$ K, the value of τ_0 is as large as $\approx 2\times 10^{-8}$ s (see Ref. 11 and 27). For lower $T \approx 0.1$ K and $n \approx 10^7$ cm^{-2}, the mobility which corresponds to the effective $\tau_0 \approx 10^{-7}$ s was observed by Shirahama *et al.*[28] In both cases, $\hbar\tau_0^{-1} \ll k_B T$. Therefore the results of the present paper fully apply to electrons on helium as long as one can disregard the inelasticity of scattering (which is very weak) and many-electron effects.

It follows from our results that the single-electron approximation does not apply to the *static* magnetoconductivity of a nondegenerate 2DES which has been measured for electrons on helium. This is in spite of the fact that, for sufficiently strong magnetic fields, the effective coupling to a short-range disorder potential becomes in some sense stronger than the electron-electron interaction. Yet it is this interaction that is responsible for the observed nonzero value of $\sigma_{xx}(0)$, at least for not too low electron densities.[14]

The role of many-electron effects for strong B is less important in the frequency range $\omega \sim \gamma$, and in particular near the peak of $\sigma_{xx}(\omega)$ which we predict. Observation of this peak and/or its counterpart in the magnetic-field dependence of the weighted ac conductivity $B^{1/2}\sigma_{xx}(\omega)$ (cf. Fig. 8) would be a clear demonstration of single-electron localization effects in quantizing magnetic fields.

ACKNOWLEDGMENTS

We are grateful to M. M. Fogler and S. L. Sondhi for valuable discussions. Work at MSU was supported by the NSF through Grant No. PHY-00071059, and by the Center for Fundamental Materials Research. L.P. was supported in part by DOE Grant No. DE-FG02-90ER40542.

APPENDIX A: GUIDING CENTER FORMALISM

Here we point out the basic expressions of the guiding center formalism needed to derive simplified expressions for the low-frequency conductivity at a given Landau level. The time evolution of the momentum operator $\mathbf{p} = -i\hbar\boldsymbol{\nabla} + (|e|/c)\mathbf{A}$ in Eq. (2) is determined by the Hamiltonian

$$H = H_0 + V(\mathbf{r}), \tag{A1}$$

where $V(\mathbf{r})$ is the scattering potential, and

$$H_0 = \hbar\omega_c \left(p_+ p_- + \frac{1}{2} \right).$$

Here $p_\pm$ are the Landau-level raising and lowering operators:

$$p_\pm = (p_x \mp i p_y)/\sqrt{2\hbar m \omega_c}, \quad [p_-, p_+] = 1.$$

The choice of signs corresponds to $B_z = -|\mathbf{B}| < 0$.

To evaluate Fourier-transformed current-current correlators like that in Eq. (2), we make a Fourier transform (over time) of the Heisenberg equations of motion for the operators p_x and p_y. This gives

$$\left[1 - \left(\frac{\omega}{\omega_c} \right)^2 \right] \langle p_\mu(t) p_\nu(0) \rangle_\omega = \frac{i\omega}{\omega_c^2} \langle \partial_\mu V(\mathbf{r}(t)) p_\nu(0) \rangle_\omega - \frac{\epsilon_{\mu\mu'}}{\omega_c} \langle \partial_{\mu'} V(\mathbf{r}(t)) p_\nu(0) \rangle_\omega, \tag{A2}$$

where ∂_μ denotes the partial derivative with respect to r_μ, the indices μ and ν enumerate the components x and y, summation over repeated indices is implied, and $\epsilon_{\mu\nu} = -\epsilon_{\nu\mu}$ is the unit antisymmetric tensor, $\epsilon_{xy} = 1$. We use the notation

$$\langle A(t) B(0) \rangle_\omega = \int_{-\infty}^{\infty} dt\, e^{i\omega t} \langle A(t) B(0) \rangle. \tag{A3}$$

The calculation can be repeated analogously for $p_\nu(0)$ in the correlators on the right-hand side of Eq. (A2). As a result, the entire current-current correlator can be expressed in terms of the correlators of the derivatives of the potential V (see, for example, Refs. 6 and 7).

In the low-frequency limit the terms containing the ratio $\omega/\omega_c \ll 1$ disappear, and the correlator of interest becomes

$$\langle p_\mu(t)p_\nu(0)\rangle_\omega = \frac{\epsilon_{\mu\mu'}\epsilon_{\nu\nu'}}{\omega_c^2}\langle \partial_{\mu'}V(\mathbf{r}(t))\partial_{\nu'}V(\mathbf{r}(0))\rangle_\omega, \quad \text{(A4)}$$

which gives a direct derivation of Eq. (12).

If the random potential $V(\mathbf{r})$ is comparatively weak, as we assume, mixing of electron states in different Landau levels by this potential is small. However, $V(\mathbf{r})$ lifts the degeneracy of each level and transforms it into a band, with a continuous energy spectrum of a width $\sim\hbar\gamma$. The low-frequency conductivity is determined by the comparatively slow intraband dynamics. Thus in Eq. (A4), in the operator $V(\mathbf{r}(t))$ we should keep only the smooth components which vary on the time scale $\gamma^{-1} \gg \omega_c^{-1}$. In this approximation we can identify

$$p_\mu(t) \to -\frac{\epsilon_{\mu\nu}}{\omega_c}\partial_\nu V(\mathbf{r}(t)) = -\frac{i\epsilon_{\mu\nu}}{\omega_c}\sum_{\mathbf{q}} q_\nu V_{\mathbf{q}} e^{i\mathbf{q}\mathbf{r}(t)}, \quad \text{(A5)}$$

where on the right-hand side one should neglect the terms that contain rapidly varying factors $\exp(in\omega_c t)$ with $n\neq 0$, associated with inter-Landau-level transitions [$V_{\mathbf{q}}$ are the spatial Fourier components of $V(\mathbf{r})$; see Eq. (7)].

The slow electron dynamics within a broadened Landau level is conveniently described by the guiding center coordinates:

$$\mathbf{R}\equiv(X,Y): \quad X = x + \frac{p_y}{m\omega_c}, \quad Y = y - \frac{p_x}{m\omega_c}.$$

The components of $\mathbf{R}$ commute with the momentum operator $[\mathbf{R},\mathbf{p}]=0$, but not with each other, $[X,Y]=-il^2$. In terms of these variables the disorder potential $V(\mathbf{r})$ can be written as

$$V(\mathbf{r}) = \sum_{\mathbf{q}} V_{\mathbf{q}} e^{i\mathbf{q}\mathbf{R} - q^2l^2/4} e^{lq_- p_+} e^{-lq_+ p_-}, \quad \text{(A6)}$$

where $q_\pm = (q_x \mp iq_y)/\sqrt{2}$. The projection of the potential V onto the Nth level is given by

$$V^{(N)}(\mathbf{r}) \equiv P_N V(\mathbf{r}) P_N = P_N \sum_{\mathbf{q}} V_{\mathbf{q}}^{(N)} e^{i\mathbf{q}\mathbf{R}}, \quad \text{(A7)}$$

$$V_{\mathbf{q}}^{(N)} = V_{\mathbf{q}} L_N(q^2l^2/2)\exp(-q^2l^2/4). \quad \text{(A8)}$$

Here $P_N = P_N^2$ is the appropriate projection operator, and $L_N(z)$ is the Nth Laguerre polynomial.

The motion projected on the Nth Landau level can be described by applying the operators P_N to the Heisenberg equation of motion for the guiding center:

$$\dot{R}_\mu(t) = -i(l^2/\hbar)\epsilon_{\mu\nu}\sum_{\mathbf{q}} q_\nu V_{\mathbf{q}} e^{i\mathbf{q}\mathbf{r}(t)}.$$

Up to a coefficient, the projected parts in the right-hand sides of this equation and Eq. (A5) coincide with each other. This shows that the projected parts of $\mathbf{p}$ and $m\dot{\mathbf{R}}$ are the same, which results in Eqs. (10) and (11). The correction to low-frequency conductivity due to inter-Landau-band transitions appear only in the second order of the perturbation theory. The corresponding contribution is suppressed by the small parameter $(\gamma/\omega_c)^2$.

APPENDIX B: CALCULATION OF FREQUENCY MOMENTS

Here we describe an efficient numerical procedure used to obtain exact expressions of high-order diagrams in expansion (31). We begin by rewriting Eq. (31) as a sum of exponentials:

$$M_{2k} = -2l^2\left(\frac{l^2}{8\pi}\right)^{k+1}\sum_{\mathcal{C}(\{\mathbf{q}\})}\sum_{\{\mathbf{b}\}}(-1)^{\sigma(\{\mathbf{b}\})} \times \int d\mathbf{q}_1 \ldots d\mathbf{q}_{2k+2}\mathcal{C}(\{\mathbf{q}\})(\mathbf{q}_1\mathbf{q}_{2k+2}) \times \exp\left(-\frac{l^2}{4}\sum_{m=1}^{2k+2} q_m^2 + i\frac{l^2}{4}\sum_{m,n=1}^{2k+2}\hat{B}_{mn}^{\{\mathbf{b}\}}\mathbf{q}_m \wedge \mathbf{q}_n\right). \quad \text{(B1)}$$

The inner sum is taken over all binary sequences $\mathbf{b}=(b_1,b_2,\ldots,b_{2k})$, with $b_i=0$ and 1. They label possible combinations of signs which arise from writing the sines in Eq. (31) in terms of exponentials. The quantity $\sigma(\{\mathbf{b}\}) \equiv \Sigma_i b_i$. The antisymmetric $(2k+2)$-dimensional square matrix $\hat{B}^{\{\mathbf{b}\}}$ has the structure

$$\hat{B}^{\{\mathbf{b}\}} = \begin{pmatrix} 0 & c_1 & c_2 & \ldots & c_{2k} & 0 \\ -c_1 & 0 & c_2 & & c_{2k} & 0 \\ -c_2 & -c_2 & 0 & & & \\ \vdots & & & \ddots & c_{2k} & \vdots \\ -c_{2k} & -c_{2k} & \ldots & -c_{2k} & 0 & \\ 0 & & & \ldots & & 0 \end{pmatrix}, \quad \text{(B2)}$$

where $c_i = (-1)^{b_i}$.

Because of the δ functions in the contraction function $\mathcal{C}(\{\mathbf{q}\})$, integration in Eq. (B1) has to be performed over $k+1$ independent wave vectors. Up to a prefactor $(\mathbf{q}_1\mathbf{q}_{2k+2})$, the integrand is an exponential of the quadratic form $(l^2/2)\Sigma\mathbf{q}_i\hat{A}_{ij}\mathbf{q}_j$, where $i,j=1,\ldots,k+1$. The matrix elements $\hat{A}_{ij}$ are themselves 2×2 matrices, $\hat{A}_{ij} = -\hat{I}\delta_{ij} + a_{ij}\hat{\sigma}_y$, where $\hat{\sigma}_y$ is the Pauli matrix, and $a_{ij} = -a_{ji} = 0, \pm 1$.

For a given contraction $\mathcal{C}(\{\mathbf{q}\})$ and a given vector $\mathbf{b}$ in Eq. (B1), i.e., for the corresponding matrix a_{ij}, the Gaussian integrals can be evaluated exactly, giving

$$I[a] = -\frac{1}{4^k}\prod_{i=1}^{k+1}(1+\lambda_i^2)^{-1/2}\sum_{m=1}^{k+1}\frac{u_{m,1}u_{m,x}^*}{1+\lambda_m^2}, \quad \text{(B3)}$$

where $i\lambda_m$ are the eigenvalues of the antisymmetric matrices a_{mn}, and $u_{m,n}$ are the components of the corresponding eigenvectors. The subscript x takes on the value $x=k+1$ if $\mathbf{q}_1$ and $\mathbf{q}_{2k+2}$ are independent variables in the pairing proce-

dure, whereas for $\mathbf{q}_1 = -\mathbf{q}_{2k+2}$ we should set $x=1$, and additionally multiply Eq. (B3) by (-1).

Given the large number of terms and the computational price of calculating the exact values in each term, we did not calculate each integral exactly. Instead, the value of a given term [specified by the choice of contraction $\mathcal{C}(\{\mathbf{q}\})$ and the binary sequence $\mathbf{b}$], was calculated numerically with double precision. With integer-valued matrices a_{ij}, the number of different values was not exceedingly large, and we used the obtained approximate values [Eq. (B3)] to assign each term to an equivalence class. The individual weights can be positive or negative, depending on the parity of $\sigma(\{\mathbf{b}\})$. This procedure was used instead of much more tedious manual classification of high-order diagrams. (In addition, we checked for several values of k that weights corresponding to special diagrams in Fig. 4 are indeed equal to zero).

After the classification of diagrams was completed, the exact value of the integral in each class was obtained by taking a representative contracted matrix a_{ij} and calculating the Gaussian integral $I[a]$ algebraically. These integrals have rational values; the final answer for M_{2k} was obtained as a weighted sum of these rational numbers with their respective bin weights. As a test, we compared the results for $k=0,1$, and 2 with explicit analytic calculation.

APPENDIX C: CONTINUED FRACTION EXPANSION

The Stieltjes transform of the conductivity $\tilde{\sigma}_c$ is defined by

$$R(z)=\frac{1}{2\pi\gamma}\int_{-\infty}^{\infty} d\omega \frac{\tilde{\sigma}_c(\omega+\omega_c)}{z-i\omega/\gamma}, \quad \mathrm{Re}\, z>0, \tag{C1}$$

while the inverse transformation has the form

$$\tilde{\sigma}_c(\omega+\omega_c)=2\lim_{\varepsilon\to 0+}\mathrm{Re}[R(\varepsilon+i\omega/\gamma)]. \tag{C2}$$

The function R is related to moments (43) by the expression

$$R(z)=\sum_{k=0}^{\infty} i^k M_k^c z^{-k-1}. \tag{C3}$$

We now construct an approximation for Eq. (C1) which applies for an even function $\tilde{\sigma}(\omega+\omega_c)=\tilde{\sigma}(-\omega+\omega_c)$, allows for the Gaussian asymptotics [Eq. (47)],

$$\lim_{\omega\to\pm\infty}\frac{\gamma^2}{\omega^2}\ln\tilde{\sigma}_c(\omega+\omega_c)=-\frac{1}{2\alpha}, \quad \alpha=\frac{3}{16}, \tag{C4}$$

and requires only a finite number of moments.

It is known[29,30] that an odd function $R(z)$ can be expanded into a Jacobi-type continued fraction,

$$R(z)=\mathrm{K}_{j=1}^{\infty}\left(\frac{\Delta_j}{z}\right), \quad \Delta_j\geqslant 0, \tag{C5}$$

where we use the notation

$$\mathrm{K}_{j=1}^{\infty}\left(\frac{\Delta_j}{z}\right)\equiv\cfrac{1}{z+\cfrac{\Delta_1}{z+\cfrac{\Delta_2}{z+\ddots}}} \tag{C6}$$

for the continued fraction with coefficients Δ_j and variable z. The first J continued-fraction coefficients $\Delta_1,\ldots,\Delta_J$ are obtained from normalized moments $M_2^c,\ldots,M_{2J}^c$ by expanding power series (C3) into the continued fraction [Eq. (C5)] using an efficient recursive algorithm.[29] Having obtained only a finite number of coefficients Δ_j, we need to estimate the remaining ones. Fortunately, the asymptotic behavior [Eq. (C4)] implies[31] the following asymptotically linear growth for the continued-fraction coefficients:

$$\lim_{j\to\infty}\frac{\Delta_j}{j}=\alpha. \tag{C7}$$

Therefore, if the first J coefficients $\Delta_1,\ldots,\Delta_J$ are found, one can then construct an approximation $R^{(J)}(z)$ to $R(z)$ by linearly continuing Δ_j for $j>J$,

$$R^{(J)}(z)=\mathrm{K}_{j=1}^{\infty}\left(\frac{\Delta_j^{(J)}}{z}\right), \tag{C8}$$

where

$$\Delta_j^{(J)}=\begin{cases}\Delta_j & \text{for} \quad j\leqslant J\\ \Delta_J+\alpha(j-J) & \text{for} \quad j>J.\end{cases} \tag{C9}$$

A continuous fraction with a linearly increasing coefficient can be written in terms of the Whittaker parabolic cylinder function D_ν,

$$T(\beta,\alpha,z)\equiv\mathrm{K}_{j=1}^{\infty}\left(\frac{\beta+\alpha j}{z}\right)=\frac{D_{-(\beta/\alpha)-1}(\alpha^{-1/2}z)}{\alpha^{1/2}D_{-\beta/\alpha}(\alpha^{-1/2}z)},$$

which is valid if $\alpha>0$, $\beta+\alpha>0$ and $\mathrm{Re}\, z>0$, so that we can write Eq. (C8) as

$$R^{(J)}(z)=\cfrac{1}{z+\cfrac{\Delta_1}{z+\ddots\cfrac{}{z+\cfrac{\Delta_{J-1}}{z+\Delta_J T(\Delta_J,\alpha,z)}}}}. \tag{C10}$$

Applying the inversion formula [Eq. (C2)] immediately gives the restored cyclotron resonance absorption $\tilde{\sigma}_c(\omega)$, as shown in Fig. 7.

*Email address: dykman@pa.msu.edu

[1] F. Wegner, Z. Phys. B: Condens. Matter **51**, 279 (1983).
[2] J.T. Chalker and P.D. Coddington, J. Phys. C **21**, 2665 (1988).
[3] B. Huckestein, Rev. Mod. Phys. **67**, 357 (1995).
[4] *Two-Dimensional Electron Systems on Helium and Other Cryogenic Substrates*, edited by E.Y. Andrei (Kluwer, Boston, 1997).
[5] E. Abrahams, S.V. Kravchenko, and M.P. Sarachik, cond-mat/0006055 (unpublished).

[6] M.I. Dykman, Phys. Status Solidi B **88**, 463 (1978); M.I. Dykman, Fiz. Nizk. Temp. **6**, 560 (1980) [Sov. J. Low Temp. Phys. **6**, 268 (1980).
[7] T. Ando, A.B. Fowler, and F. Stern, Rev. Mod. Phys. **54**, 437 (1982).
[8] R.W. van der Heijden, M.C.M. van de Sanden, J.H.G. Surewaard, A.T.A.M. de Waele, H.M. Gijsman, and F.M. Peeters, Europhys. Lett. **6**, 75 (1988).
[9] P.W. Adams and M.A. Paalanen, Phys. Rev. B **37**, 3805 (1988).
[10] P. Scheuzger, J. Neuenschwander, W. Joss, and P. Wyder, Physica B **194-196**, 1231 (1994).
[11] M.J. Lea, in *Two-Dimensional Electron Systems on Helium and Other Cryogenic Substrates* (Ref. 4), p. 125.
[12] M.J. Lea and M.I. Dykman, Physica B **251**, 628 (1998), and references therein.
[13] E. Teske, Yu.P. Monarkha, M. Seck, and P. Wyder, Phys. Rev. Lett. **82**, 2772 (1999).
[14] F. Kuehnel, L.P. Pryadko, and M.I. Dykman, cond-mat/0001427 (unpublished).
[15] L.B. Ioffe and A.I. Larkin, Zh. Éksp. Teor. Fiz. **81**, 1048 (1981) [Sov. Phys. JETP **54**, 556 (1981)].
[16] K.A. Benedict, Nucl. Phys. B **280**, 549 (1987).
[17] B.I. Halperin and M. Lax, Phys. Rev. **148**, 722 (1966); J. Zittartz and J.S. Langer, *ibid.* **148**, 741 (1966).
[18] Details of the calculations and more detailed results can be found in F. Kuehnel, Ph.D. thesis, Michigan State University, 2000.
[19] B. Mieck, Europhys. Lett. **13**, 453 (1990).
[20] J.T. Chalker and G.J. Daniell, Phys. Rev. Lett. **61**, 593 (1988).
[21] Z.-Q. Wang, M. P.A. Fisher, S.M. Girvin, and J.T. Chalker, Phys. Rev. B **61**, 8326 (2000).
[22] S. L. Sondhi (unpublished).
[23] See, for example, A.M. Stoneham, *Theory of Defects in Solids: Electronic Structure of Defects in Insulators and Semiconductors* (Clarendon Press, Oxford, 1975).
[24] http://www.mathsource.com/Content/Enhancements/ Calculus/ 0211-138
[25] M. Böhm, K. Broderix, and H. Leschke, Z. Phys. B: Condens. Matter **104**, 111 (1997).
[26] M. Saitoh, Solid State Commun. **52**, 63 (1987).
[27] M.J. Lea, P. Fozooni, A. Kristensen, P.J. Richardson, K. Djerfi, M.I. Dykman, C. Fang-Yen, and A. Blackburn, Phys. Rev. B **55**, 16 280 (1997), and references therein.
[28] K. Shirahama, S. Ito, H. Suto, and K. Kono, J. Low Temp. Phys. **101**, 439 (1995).
[29] H.S. Wall, *Continued Fractions* (Van Nostrand, New York, 1948).
[30] O. Perron, *Die Lehre von Kettenbrüchen* (Teubner, Stuttgart, 1977), Vols. I and II.
[31] D.S. Lubinksy, H.N. Mhaskar, and E.B. Saff, Constr. Approx. **4**, 65 (1988).